Available online at www.sciencedirect.com
ScienceDirect
Earth and Planetary Science Letters 258 (2007) 307–314
EPSL
www.elsevier.com/locate/epsl

Limits on rock strength under high confinement

Carl E. Renshaw [a,*], Erland M. Schulson [b,1]

[a] Department of Earth Sciences, Dartmouth College, Hanover, NH 03755, United States
[b] Thayer School of Engineering, Dartmouth College, Hanover, NH 03755, United States

Received 25 October 2006; received in revised form 23 March 2007; accepted 25 March 2007
Available online 1 April 2007
Editor: G.D. Price

Abstract

Understanding of deep earthquake source mechanisms requires knowledge of failure processes active under high confinement. Under low confinement the compressive strength of rock is well known to be limited by frictional sliding along stress-concentrating flaws. Under higher confinement strength is usually assumed limited by power-law creep associated with the movement of dislocations. In a review of existing experimental data, we find that when the confinement is high enough to suppress frictional sliding, rock strength increases as a power–law function only up to a critical normalized strain rate. Within the regime where frictional sliding is suppressed and the normalized strain rate is below the critical rate, both globally distributed ductile flow and localized brittle-like failure are observed. When frictional sliding is suppressed and the normalized strain rate is above the critical rate, failure is always localized in a brittle-like manner at a stress that is independent of the degree of confinement. Within the high-confinement, high-strain rate regime, the similarity in normalized failure strengths across a variety of rock types and minerals precludes both transformational faulting and dehydration embrittlement as strength-limiting mechanisms. The magnitude of the normalized failure strength corresponding to the transition to the high-confinement, high-strain rate regime and the observed weak dependence of failure strength on strain rate within this regime are consistent with a localized Peierls-type strength-limiting mechanism. At the highest strain rates the normalized strengths approach the theoretical limit for crystalline materials. Near-theoretical strengths have previously been observed only in nano- and micro-scale regions of materials that are effectively defect-free. Results are summarized in a new deformation mechanism map revealing that when confinement and strain rate are sufficient, strengths approaching the theoretical limit can be achieved in cm-scale sized samples of rocks rich in defects. Thus, non-frictional failure processes must be considered when interpreting rock deformation data collected under high confinement and low temperature. Further, even at higher temperatures the load-bearing ability of crustal rocks under high confinement may not be limited by a frictional process under typical geologic strain rates.

Keywords: fracture; high confinement; Peierls; creep

1. Introduction

Understanding failure processes under high confinement is important due to their possible role as deep earthquake source mechanisms [e.g., 1,2]. It is well established that under low confinement, low temperature, and high strain rate, compressive failure of intact rock is

* Corresponding author. Tel.: +1 603 646 3365; fax: +1 603 646 3922.
E-mail addresses: Carl.Renshaw@Dartmouth.edu (C.E. Renshaw), Erland.Schulson@Dartmouth.edu (E.M. Schulson).
[1] Tel.: +1 603 646 2888; fax: +1 603 646 3856.

0012-821X/$ - see front matter © 2007 Elsevier B.V. All rights reserved.
doi:10.1016/j.epsl.2007.03.043

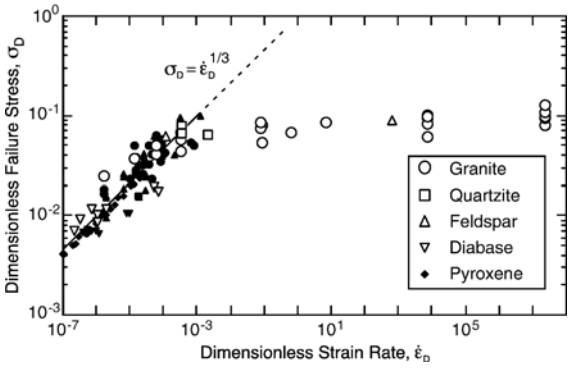

Fig. 1. Observed failure stress and mode in various rock types strained under high confinement. Filled symbols indicate failure by globally distributed ductile flow, open symbols brittle-like faulting. Data sources as cited in Table 1.

associated with the initiation and sliding of microcracks [3–6], with terminal failure occurring through the localization of damage along a fault oriented at an acute angle to the greatest compressive stress [7,8]. The orientation of the fault and the strength of the material are consistent with the dictates of internal friction, and so this process has been termed Coulombic faulting [6].

Because Coulombic faulting depends upon crack sliding, this mode of failure is suppressed when the shear stress is not sufficient to overcome the frictional resistance to sliding along microcracks. This happens under triaxial loading when the confinement ratio $R \equiv \sigma_3/\sigma_1$ is increased beyond a critical level, R_c, defined by [5]

$$R_c = \frac{(1+\mu^2)^{0.5} - \mu}{(1+\mu^2)^{0.5} + \mu}. \quad (1)$$

where μ is the coefficient of internal friction.

Mineralogic changes (i.e., dehydration embrittlement [9] or transformational faulting [10]) are well established high confinement faulting mechanisms. Here we review existing experimental rock failure data collected under high confinement and find that other mechanisms also result in brittle-like failure under high confinement. In particular, we find that above a critical normalized strain rate, failure is always localized in a brittle-like manner at a stress that is independent of degree of confinement. At the highest strain rates the normalized strengths approach the theoretical limit for crystalline materials. The results highlight the broad suite of non-Coulombic brittle-like failure mechanisms possible under high confinement.

2. Experimental data

In Fig. 1 we summarize experimentally observed failure stresses determined from triaxial compression tests on cm-scale cores of a variety of rock types. This figure only includes experiments in which the confinement was sufficient to suppress frictional sliding ($R > R_c = 0.3$), assuming a typical value of the coefficient of friction $\mu = 0.6$ [11]. Filled symbols indicate failure by globally distributed ductile flow; open symbols indicate that terminal failure occurred in a brittle-like manner with deformation localized along a discrete macroscopic fault inclined to the direction of maximum compression. The data show that highly confined rock exhibits quite pronounced strain-rate hardening at lower (dimensionless) strain rates, but only weak strain-rate hardening at higher strain rates. At the transition, the (dimensionless) strength is about 0.04 G, where G is the shear modulus.

Within the lower-rate regime, observed failure stresses agree well with those predicted for power-law or dislocation creep, where failure stress is given by the expression

$$\sigma_D = \dot{\varepsilon}_D^{1/n} \quad (2)$$

where $\sigma_D = (\sigma_1 - \sigma_3)/G$, where σ_1 and σ_3 are the most compressive and the least compressive principal stresses,

Table 1
Rock parameters

Rock	G (MPa)	ν	Log A [a] (MPa^{-n} s^{-1})	Q [a] (kJ/mol)	R_c	T (°C)	d/b	σ_P/G (Eq. (5))
Granite [8,44,45]	23800	0.24	−8.9	100	0.30–0.55	25–300	0.615 [b]	0.21
Quartzite [46]	38700	0.09	−9.4	99	0.30–0.33	500–600	0.55	0.33
Feldspar [47]	38700	0.30	−8.9	65	0.30–0.33	25	0.58	0.21
Diabase [16]	40900	0.24	−1.21	276	0.30–0.46	970–1030	0.714	0.14
Pyroxene [48]	40700	0.21	−2.2	290	0.48–0.86	950–1300	0.714	0.15
Olivine [32]	64300	0.26	−6	523	–	118–773	0.714	0.13

Elastic constants are as reported by Birch [49] and Christensen [50].
Lattice spacings as reported by Wang and Nieh [51] and Wang [52].
[a] Creep parameters are best fits assuming $n = 3$ Parameters estimated for Olivine.
[b] Average of feldspar, quartz, and biotite lattice spacings.

respectively. The dimensionless strain rate is defined as $\dot{\varepsilon}_D = \dot{\varepsilon}/(BG^n)$, where $\dot{\varepsilon}$ is the applied strain rate and $B = Ae^{-Q/RT}$, where A is a materials constant, Q is the activation energy, T is the absolute temperature and R is the gas constant. The value of the stress exponent for rock [12] is typically $n \sim 3$. Parametric values are listed in Table 1. While the dimensionless strain rates for these experiments span 14 orders of magnitude, the actual strain rates vary over a considerably smaller range (generally of order 10^{-5} to 10^{-6} s^{-1}). The great variation in dimensionless strain rates reflects both the wide range of experimental temperatures (25–1300 °C) and the significant variation in creep parameters amongst rock types.

Within the lower-rate regime two distinct modes of macroscopic failure are evident: distributed ductile failure, as expected for power–law creep, and localized, brittle-like failure. The latter mode is observed over the entire range of dimensionless strain rates. The character of the faults forming under high confinement ($R > R_c$) is different from those of Coulombic faults occurring when $R < R_c$. While Coulombic faults generally form at an angle $\theta \sim 30°$ to the greatest principal stress, high-R faults of the kind that limit the strength of the rock cited in Fig. 1 are oriented at higher angles ($\theta \sim 40$–$45°$), sub-parallel to the plane of maximum shear stress ($\theta = 45°$) and consistent with the activation of plastic flow processes [13]. Also, in comparison to Coulombic faults, high-R faults are very narrow (<1 μm). Judging from the lack of a significant increase in acoustic emissions prior to failure [14] and from photomicrographs of these high-R faults [15], the total amount of damage associated with their formation is significantly less than for Coulombic faults. And the specific type of damage differs: absent in grains adjacent to high-R faults [14–16] are the closely spaced "axial" or "mode I" microcracks common in Coulombic faulting (e.g., [17]).

The consistency of the observed trend in failure strengths across a variety of rock types and mineralogies argues against either dehydration embrittlement [9] or transformational faulting [10] as the strength limiting mechanism for these data. Instead, we have argued elsewhere [18,19] that brittle-like failure may occur under high confinement when strain is localized due to a plastic instability that develops when thermal softening exceeds both strain hardening and strain-rate hardening [20]. In that case, and as observed for these data, the predicted terminal failure stress follows a power law similar to Eq. (2) (see Eq. (5) in [18]). Alternatively, Main [21] has shown that localized failure can occur within the power-law creep regime at long times due to the co-existence and interaction of both negative (softening) and positive (hardening) mechanisms active during creep deformation. Thus for dimensionless strain rates $\dot{\varepsilon}_D < \sim 10^{-4}$ the data in Fig. 1 are consistent with existing theories: both dislocation creep and plastic faulting predict a power–law relationship between dimensionless strain rate and terminal failure stress, as observed. It remains unclear, however, what causes distributed creep in some cases and plastic faulting in others.

Above dimensionless strain rates of $\dot{\varepsilon}_D \sim 10^{-4}$ only localized brittle-like failure occurs. In this high-R, high-$\dot{\varepsilon}_D$ regime, terminal failure stresses are only weakly dependent on dimensionless strain rate, as already noted, and the terminal failure stress is no longer governed by the power law in Eq. (2). What mechanism limits strength within this regime? Again the consistency of the data across differing rock types and mineralogies argues against dehydration embrittlement or transformational faulting. Furthermore, the mean stress at failure for the faulted granite samples in Fig. 1 varies by more than a factor of three, and the samples were deformed at temperatures ranging from ambient to 900 °C. This implies the absence of a critical mean stress or temperature that would be expected for faulting associated with mineralogic phase transitions. We consider below alternative possibilities: Mode-II sliding, the Peierls mechanism, and the theoretical shear strength.

3. High confinement, high strain rate brittle-like failure mechanisms

3.1. Mode II fracture

Several authors have noted a change in the character of brittle-like failure with increasing temperature [13] or

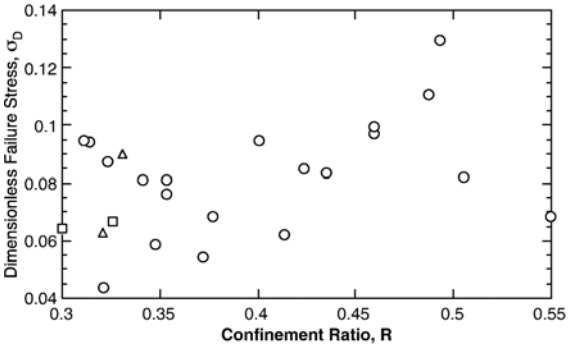

Fig. 2. Failure stress for high confinement, high strain rate brittle-like faulting versus confinement. Symbol key is the same as for Fig. 1. Best linear least squares fit ($r^2 = 0.07$) to the data (not shown) has a slope of 0.086±0.099 (best fit slope±twice standard error), i.e., not significantly different from zero.

confinement [15]. Hirth and Tullis [15] argue that the change from Coulombic-type faults under low confinement to more narrow faults associated with less damage and with an absence of axial microcracks is due to a transition from dominantly mode I microcracking under low confinement to dominantly mode II type microcracking under high confinement. Mode II type fracture requires the propagation of a stress singularity created by a shear displacement discontinuity at the fracture tip. If the shear displacement discontinuity is created by frictional sliding, then we would expect the differential stress at terminal failure to increase with increasing confinement, as predicted, for example, by Byerlee's law [11]. However, consistent with the suppression of frictional sliding predicted by Eq. (1), for the high-R, high-$\dot{\varepsilon}_D$ faults there is no significant increase in differential failure stress with increasing confinement ratio (Fig. 2). For this figure, the best linear least squares fit (r_2=0.11) to the data (not shown) has a slope of 0.09±0.1 (best fit slope±twice standard error), i.e., not significantly different from zero.

Frictional sliding might occur without an increase in terminal failure stress if there is a corresponding decrease in the coefficient of friction due to increasing temperature or pressure [22]. The required decrease in friction is significant: the high strain rate ($\dot{\varepsilon}_D > 10^{-4}$) faults in Fig. 1 occurred under confinements as high as R=0.55, which corresponds to a coefficient of friction of μ=0.3 (Eq. (1)) — significantly lower than the values typical for rock (μ=0.6–0.8) [11]. And many of the faults in Fig. 1 occurred at temperatures <500 °C: below this temperature the coefficient of friction for sliding along granite surfaces has been shown to be independent of temperature [11,23]. Furthermore, Hirth and Tullis [15] noted that what they refer to as mode II type fractures occur even at room temperature, implying that only an increase in confining pressure, and not temperature, is sufficient to permit high-R, high-$\dot{\varepsilon}_D$ type fracture. There is little conclusive evidence for a pressure dependent decrease in the coefficient of friction, at least for confining pressures less than ~GPa [24,25]. Thus, the high-R, high-$\dot{\varepsilon}_D$ faults depicted in Fig. 1 do not appear to be consistent with Mode-II type fracture as the strength limiting process.

3.2. Peierls mechanism

Ohnaka [13] noted that the increase in fault angle with increasing confinement is consistent with the activation of plastic flow processes. Thus the growth of the high-R, high-$\dot{\varepsilon}_D$ faults in Fig. 1 may be controlled by the localization of plastic flow along a discrete plane — a process analogous to the mechanism of plastic faulting [18,19].

The weak strain rate dependence of the brittle-like failure strength for the high-R, high-$\dot{\varepsilon}_D$ faults shown Fig. 1 argues against the localized plastic failure being governed by power–law creep (Eq. (2)). This is not surprising given the high stress conditions under which these faults form. Numerous authors [26–28] have previously noted that the creep power–law breaks down for silicate rocks at stress levels $\sigma_D > \sim 10^{-2}$. As already noted, the transition to high-R, high-$\dot{\varepsilon}_D$ faulting occurs at a similar stress (Fig. 1). Stocker and Ashby [28] attribute the break-down of power law creep at $\sigma_D \sim 10^{-2}$ to a transition in the primary deformation mechanism from dislocation creep to thermally activated dislocation glide controlled by lattice-resistance; i.e., to a strength limiting mechanism governed by the stress required to overcome the Peierls barrier to dislocation glide. Conversely, the observed change in failure mechanism, as indicated by the break in slope of the curve in Fig. 1 circa σ_D of the order 10^{-2}, is consistent with the strength limiting mechanism in these samples transitioning from dislocation creep to dislocation glide.

Evans and Goetze [29] have argued that the fully plastic deformation of olivine underneath a microindenter is controlled by the Peierls mechanism and is governed by a flow law of the form [30,31]

$$\dot{\varepsilon} = A_p e^{\frac{-\Delta E}{RT}} \tag{3}$$

where A_p is assumed to be a constant and ΔE is the free energy of activation of slip. The form of the free energy function depends on the shape of the energy barrier to dislocation glide, and has been described phenomenologically by Kocks et al. [30] through the relationship:

$$\Delta E = Q_P \left[1 - \left(\frac{(\sigma_1 - \sigma_3)}{\sigma_P}\right)^p\right]^q \tag{4}$$

where Q_P is the activation enthalpy and σ_P is the Peierls stress at 0° K and where the exponents fall within the range $0 < p \leq 1$ and $1 < q < 2$. Following Evans and Goetze [32] we initially set p=1 and q=2. Later we explore the sensitivity of our results to these values.

Huntington [33] has shown that the Peierls stress can be estimated as

$$\frac{\sigma_P}{G} \approx \frac{2}{1-\nu} e^{\frac{-\pi}{(1-\nu)}(d/b)} \tag{5}$$

where ν is Poisson's ratio, d is the distance between slip planes and b is the distance between atoms in the slip direction. Slight modifications to Eq. (5) have been proposed (e.g., [34]), but as noted below we find the

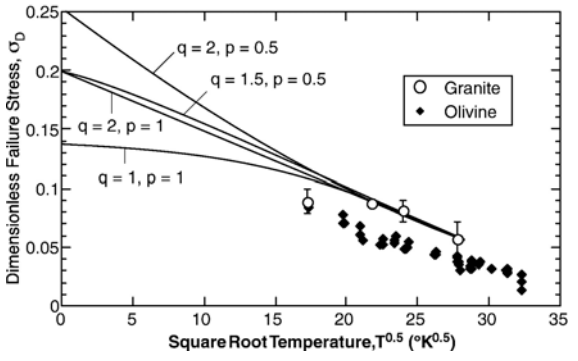

Fig. 3. Observed failure stress for granite ($\dot{\varepsilon}D > 10^{-4}$) and olivine under high confinement and high dimensionless strain rate versus temperature. Data sources as cited in Table 1. Error bars, when shown, indicate ± twice the standard error of samples tested at same temperature.

above approximation to be consistent with the data discussed here. Peierls stresses calculated using Eq. (5) are included in Table 1.

Eqs. (3) and (4) can be rewritten as [32]

$$\sigma_D = \frac{\sigma_P}{G} + m_P\sqrt{T} \tag{6}$$

where

$$m_P = \frac{\sigma_P}{G}\sqrt{\frac{R\ \ln(A_P/\dot{\varepsilon})}{Q_P}} \tag{7}$$

Accordingly, the brittle-like failure strength for the high-R, high-$\dot{\varepsilon}_D$ faults in granite from Fig. 1 are re-plotted in Fig. 3 as a function of $\sqrt{T}$ along with the olivine yield stresses determined using micro-indentation hardness [32]. For the granite data we plot, at each temperature, the mean observed failure stress and, when possible, error bars indicating the standard error about the mean. Thus these data represent far more than just four experiments. Excluding the lowest temperature data for the granite (more below), the agreement between the experimental data for both rock types and a fit of the form of Eq. (6) is good ($p=1$, $q=2$). (To simplify this figure, the fit for the olivine data is not shown, but the fit curve is nearly identical to that for the granite but offset along the y-axis. Fits to the olivine data are shown in Fig. 15 of Evans and Goetze [32]). Furthermore, we note that the Peierls stress extrapolated from the fit to the granite data in Fig. 3 ($\sigma_p/G=0.20$) is in good agreement with that predicted using Eq. (5) ($\sigma_p/G=0.21$). Similarly good agreement is found between the Peierls stress extrapolated from a best fit ($p=1$, $q=2$) to the experimental data for olivine ($\sigma_p/G=0.14$) and the theoretical estimate ($\sigma_p/G=0.13$) [32]. Because all tests on each rock type were done at the same strain rate, it is not possible to independently determine A_P and Q_P from these data.

Fig. 3 shows that equally good fits to the data are possible using any combination of exponents within the ranges $0.5 < p \leq 1$ and $1 < q < 2$. Extrapolated Peierls stresses are somewhat sensitive to the values of the exponents, but still remain in reasonable agreement with those estimated using Eq. (5). We conclude that while it is not possible to determine the appropriate values of the exponents from the data, the model results are not highly sensitive to these values. It is convenient, therefore, to take advantage of the analytical simplicity provided by the mid-range estimates of $p=1$ and $q=2$.

We conclude that with the exception of the lowest temperature faults in granite (more below), the failure strengths associated with the high-R, high-$\dot{\varepsilon}_D$ faults in Fig. 1 appear to be consistent with a Peierls-type mechanism governing the brittle-like failure. However, some caution in this interpretation is warranted. Microstructural analyses of the region in the olivine under the indenter where the Peierls mechanism is thought to govern deformation are consistent with distributed plastic flow, i.e., they do not reveal regions of localized deformation as seen in the larger granite samples. If the Peierls mechanism similarly limits the strength of triaxially-compressed granite under high-R, high-$\dot{\varepsilon}_D$ conditions, why then is failure localized in the granite but not in the olivine?

A possible explanation for this difference in failure modes follows from the analysis of plastic faulting presented by Renshaw and Schulson [18]. They note that localized deformation along a plastic-like fault can only be maintained when the shear strain rate within the shear zone is sufficient to maintain near-adiabatic conditions. The required shear strain rate within the shear zone is given by (Eq. (4) in [18]):

$$\left(\frac{\partial\gamma}{\partial t}\right)_c \approx \frac{-m\kappa}{(\partial\tau_o/\partial T)r_c^2} \tag{8}$$

where κ is the thermal conductivity, r_c is a characteristic dimension for the sample (e.g., the radius of a cylindrical sample), τ_o is the maximum shear stress at terminal failure, and m is the work-hardening exponent in the power–law stress–strain relationship $\tau_o = \beta\gamma^m$ where β is a constant. Taking the scale of the indents in olivine ($\sim 10^{-5}$ m) as the characteristic dimension, differentiating Eq. (6) to obtain $\partial\tau_o/\partial T = Gm_P/(4\sqrt{T})$, which has a typical value of ~ 2 MPa $K^{-0.5}$ (Fig. 3), and assuming the remaining parameters are similar to those for granite ($m=0.3$, $\kappa \sim 2$ W/(mK) [18]), the required strain rate for

localization in the olivine under the indenter is $\sim 10^3$ s^{-1}. This is about eight orders of magnitude greater than the effective strain rate in these tests. In contrast, taking the scale of the granite samples (1 cm) as the characteristic dimension, the required strain rate within the shear zone is $\sim 10^{-2}$ s^{-1}. The corresponding global strain rate, obtained by multiplying the local strain rate by $L_z/(2L)$, where L is the length of the sample (~ 1 cm) and L_z is the width of the incipient shear zone (~ 1 μm), is 10^{-7} s^{-1}, or about an order of magnitude lower than the applied strain rate in tests (10^{-6} s^{-1}). Thus only in the granite samples was the strain rate sufficient to support localization through adiabatic heating.

3.3. Theoretical strength

Fig. 3 shows that the strengths of the granite samples at 300 K fall significantly below the curve extrapolated from the higher temperature granite data even when the standard errors in these data are taken into account. Comparing the predicted model fits (solid lines, Fig. 3) for the failure stress at this temperature (~ 0.12 regardless of the values of p and q) to the mean and standard error of the data at this temperature, a t-test indicates that the model and experimental data are significantly different at the $p \ll 0.001$ level. Still, one may choose to argue that the number of available data is small and the lack of fit of no significance. On the other hand, we note that the level of stress at which this deviation from the Peierls curve occurs is close to the theoretical strength of rock (given below) where the failure stress is governed by the shear rupture of atomic bonds across a slip plane. Perhaps, then, the deviation marks the onset of terminal failure at the theoretical limit? Should the latter possibility be correct, we would expect that the strength at still lower temperatures would remain at this level. We would also expect that other materials would show a similar deviation at sufficiently low temperatures. Unfortunately, the data are too limited to test this idea further. And the technical challenges involved in obtaining the data at the necessary temperatures are significant.

In claiming that the strength of cold rock appears to approach the theoretical limit, what do we take as the theoretical shear strength? Estimates of this limit depend upon the assumed atomic structure. Early estimates were based on the rigid sphere model of atoms [35,36], but were later modified to account for the compressibility of atoms and the effect of local charge transfers [37]. More recently, *ab initio* calculations using density function theory have permitted quantitatively rigorous evaluations of the theoretical shear strength [e.g., 38]. But *ab initio* evaluations are only valid for perfect crystals under uniform deformation and cannot be employed for cases of non-uniform deformation or bodies of inhomogeneous microstructures such as rocks. Nonetheless, results from these theoretical studies are generally consistent with recent experimental studies that examine very small scale regions of material that are essentially defect-free [38–41]. The results can be summarized by noting that the theoretical shear strength is usually well approximated by an expression of the form

$$\sigma_{\mathrm{D}}^{Th} \approx k \tag{9}$$

where k is a constant of order 10^{-1}. For example, with the rigid sphere model $k \approx b/(2\pi a)$, where b is the distance between atoms in the slip direction and a is the spacing between adjacent lattice planes [35]. When the compressibility of atoms is accounted for [42] $k \approx 1/15$ and when local charge transfers are accounted for [37] $k \approx 1/20$. This range of variation in estimated values of k is similar to the variation in k determined experimentally [38–41]. Taking as an approximate upper bound estimate $k \sim 0.1$, we find that the failure strength of the coldest granite samples in Fig. 3 is similar to the estimated theoretical strengths. Hence, we wonder if in these experiments the failure strength may have been limited by shear rupture at the theoretical limit. The reason a similar deviation from linearity is not observed in the olivine data may be that the range of temperature did not include sufficiently low temperatures for the failure strength to approach σ_{D}^{Th}.

While the mechanisms of brittle-like failure limiting strength for $\dot{\varepsilon}_{\mathrm{D}} > \sim 10^{-4}$ remain uncertain, the data clearly demonstrate that failure stresses can approach the theoretical strength, even in cm-scale specimens of rock rich in defects. This result is novel in that strengths approaching the theoretical limit have previously only been recognized in very small scale, essentially defect-free materials or within nearly defect-free, nano-scale regions of materials.

4. Discussion and conclusions

The compressive failure strength of a variety of rocks triaxially loaded under confinement high enough to suppress frictional sliding is independent of the degree of confinement and exhibits a transition from relatively strong to relatively weak dependence upon strain rate once the normalized strain rate reaches $\dot{\varepsilon}_{\mathrm{D}} \sim 10^{-4}$. The strength at the transition reaches ~ 0.04 G, and then approaches ~ 0.1 G at the highest rates for which data are available. We attribute this transition to a change in

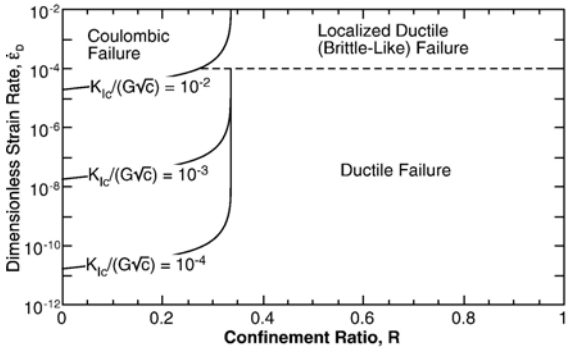

Fig. 4. Deformation mechanism as a function of confinement and strain rate.

the fundamental mechanism of deformation limiting strength, from one controlled by dislocation creep at lower strain rates to one controlled by overcoming the Peierls barrier to dislocation glide at higher strain rates. We suggest that at the highest strain rates, the strength approaches the theoretical shear strength of the material.

In previous work we found that the strain rate $\dot{\varepsilon}_D^{\text{Transition}}$ at which the failure mechanism transitions from brittle Coulombic to ductile is well approximated as

$$\dot{\varepsilon}_D^{\text{Transition}} \approx \left(\frac{K_{Ic}}{G\sqrt{c}}\right)^n \frac{9}{(1-R)-\mu(1+R)} \qquad (10)$$

where K_{Ic} is the mode I critical stress intensity factor for crack growth and c is half the characteristic grain size. Note that the value of the constant in the above expression reflects the correction of a minor algebraic error in the original work. Combining this brittle to ductile transition with the transition to localized ductile failure reported here for $\dot{\varepsilon}_D > \sim 10^{-4}$ results in the generalized deformation mechanism map shown in Fig. 4.

Our findings imply that it should be possible to observe failure strengths close to the theoretical limits in other defect-rich materials if the confinement and applied strain rate are sufficiently high. For aluminum and other face-centered cubic metals [43] at a homologous temperature ~ 0.5, the required strain rates ($\sim 10^6$ s^{-1}) are not common in geologic processes. However, using the parameters in Table 1, the strain rate required for localized (brittle-like) ductile failure for pyroxene and olivine, two common lower crust minerals, are of the order 10^{-10} s^{-1} and 10^{-27} s^{-1} at the same homologous temperature (~ 600 °C). These strain rates bracket the range of typical geological strain rates [12], suggesting that in some cases the load-bearing ability of crustal rocks under high confinement may not be limited by a frictional process.

Acknowledgements

We gratefully acknowledge the helpful comments of the reviewer of the initial version of this manuscript. This work was partially supported by the U.S. National Science Foundation, grant nos. ARC-0520375 and OPP-0328605.

References

[1] R. Tibi, G. Bock, D.A. Wiens, Source characteristics of large deep earthquakes: constraint on the faulting mechanism at great depths, J. Geophys. Res., [Solid Earth] 108 (2003).
[2] C.H. Estabrook, Seismic constraints on mechanisms of deep earthquake rupture, J. Geophys. Res., [Solid Earth] 109 (2004).
[3] W.F. Brace, E.G. Bombolakis, A note on brittle crack growth in compression, J. Geophys. Res. 68 (1963) 3709–3713.
[4] H. Horii, S. Nemat-Nasser, Brittle failure in compression: splitting, faulting, and brittle–ductile transition, Philos. Trans. R. Soc. Lond., A 319 (1986) 337–374.
[5] M.F. Ashby, S.D. Hallam, The failure of brittle solids containing small cracks under compressive stress states, Acta Metall. 34 (1986) 497–510.
[6] C.E. Renshaw, E.M. Schulson, Universal behaviour in compressive failure of brittle materials, Nature 412 (2001) 897–900.
[7] D.A. Lockner, J.D. Byerlee, V. Kuksenko, A. Ponomarev, A. Sidorin, Quasi-static fault growth and shear fracture energy in granite, Nature 350 (1991) 39–42.
[8] M. Shimada, Confirmation of two types of fracture in granite deformed at temperatures to 300 °C, Tectonophysics 211 (1992) 259–268.
[9] C. Meade, R. Jeanloz, Deep focus earthquakes and recycling of water into the Earth's mantle, Science 252 (1991) 68–72.
[10] S.H. Kirby, Localized polymorphic phase transformations in high-pressure faults and applications to the physical mechanism of deep earthquakes, J. Geophys. Res. 92 (1987) 13,789–13,800.
[11] J.D. Byerlee, Friction of rocks, Pure Appl. Geophys. 116 (1978) 615–626.
[12] N.L. Carter, M.C. Tsenn, Flow properties of continental lithosphere, Tectonophysics 136 (1987) 27–63.
[13] M. Ohnaka, A shear failure strength law of rock in the brittle-plastic transition regime, Geophys. Res. Lett. 22 (1995) 25–28.
[14] M. Shimada, Confirmation of 2 types of fracture in granite deformed at temperatures to 300-degrees-C, Tectonophysics 211 (1992) 259–268.
[15] G. Hirth, J. Tullis, The brittle-plastic transition in experimentally deformed quartz aggregates, J. Geophys. Res., [Solid Earth] 99 (1994) 11731–11747.
[16] Y. Caristan, The transition from high-temperature creep to fracture in Maryland diabase, J. Geophys. Res. 87 (1982) 6781–6790.
[17] P. Tapponnier, W.F. Brace, Development of stress-induced microcracks in Westerly Granite, Int. J. Rock Mech. Min. Sci. 13 (1976) 103–112.
[18] C.E. Renshaw, E.M. Schulson, Plastic faulting: brittle-like failure under high confinement, J. Geophys. Res., [Solid Earth] 109 (2004) B09207.

[19] E.M. Schulson, Compressive shear faults in ice: plastic vs Coulombic faults, Acta Mater. 50 (2002) 3415–3424.
[20] B.E. Hobbs, A. Ord, Plastic instabilities; implications for the origin of intermediate and deep focus earthquakes, J. Geophys. Res. B, [Solid Earth Planets] 93 (1988) 10,521–10,540.
[21] I.G. Main, A damage mechanics model for power–law creep and earthquake aftershock and foreshock sequences, Geophys. J. Int. 142 (2000) 151–161.
[22] G.L. Shelton, J. Tullis, T. Tullis, Experimental high-temperature and high-pressure faults, Geophys. Res. Lett. 8 (1981) 55–58.
[23] R.M. Stesky, W.F. Brace, D.K. Riley, P.-Y.F. Robin, Friction in faulted rock at high temperature and press, Tectonophysics 23 (1974) 177–203.
[24] J.D. Byerlee, Frictional characteristics of granite under high confining pressure, J. Geophys. Res. 72 (1967) 3639–3648.
[25] A. Kato, M. Ohnaka, H. Mochizuki, Constitutive properties for the shear failure of intact granite in seismogenic environments, J. Geophys. Res., [Solid Earth] 108 (2003).
[26] C. Goetze, The mechanisms of creep in olivine, Philos. Trans. R. Soc. Lond., A 288 (1978) 99–119.
[27] R.J.J. Post, High-temperature creep of Mt. Burnet dunite, Tectonophysics 42 (1977) 75–110.
[28] R.L. Stocker, M.F. Ashby, On the rheology of the upper mantle, Rev. Geophys. 11 (1973) 391–497.
[29] C. Goetze, B. Evans, Stress and temperature in the bending lithosphere as constrained by experimental rock mechanics, Geophys. J. R. Astro. Soc. 59 (1979) 463–478.
[30] U.F. Kocks, A.S. Argon, M.F. Ashby, Thermodynamics and kinetics of slip, Prog. Mater. Sci. 19 (1975) 1–281.
[31] J.E. Dorn, S. Rajnak, Nucleation of kink pairs+Peierls mechanism of plastic deformation, Trans. Metall. Soc. AIME 230 (1964) 1052–1074.
[32] A.G. Evans, C. Goetze, The temperature variation of hardness of olivine and its implication for polycrystalline yield stress, J. Geophys. Res. 84 (1979) 5505–5524.
[33] H.B. Huntington, Modification of the Peierls–Nabarro model for edge dislocation core, Proc. Phys. Soc. London, Sect. B 68 (1955) 1043–1048.
[34] J.N. Wang, A new modification of the formulation of Peierls stress, Acta Mater. 44 (1996) 1541–1546.
[35] J. Frenkel, Zur theorie der elastizitätsgrenze und der festigkeit kristallinischer körper, Z. Phys. 37 (1926) 572–609.
[36] A. Kelly, Strong Solids, Oxford University Press, New York, 1973.
[37] H. Fujita, N. Fujita, Heterogeneous deformation and mechanical strength of materials — approach to the theoretical strength, Radiat. Eff. Defects Solids 157 (2002) 85–100.
[38] S. Ogata, J. Li, S. Yip, Ideal pure shear strength of aluminum and copper, Science 298 (2002) 807–811.
[39] H. Bei, Z.P. Lu, E.P. George, Theoretical strength and the onset of plasticity in bulk metallic glasses investigated by nanoindentation with a spherical indenter, Phys. Rev. Lett. 93 (2004).
[40] J. Chen, W. Wang, L.H. Qian, K. Lu, Critical shear stress for onset of plasticity in a nanocrystalline Cu determined by using nanoindentation, Scr. Mater. 49 (2003) 645–650.
[41] A. Gouldstone, H.J. Koh, K.Y. Zeng, A.E. Giannakopoulos, S. Suresh, Discrete and continuous deformation during nanoindentation of thin films, Acta Mater. 48 (2000) 2277–2295.
[42] A.H. Cottrell, Dislocations and Plastic Flow in Crystals, Oxford University Press, New York, 1953.
[43] H.J. Frost, M.F. Ashby, Deformation-Mechanism Maps, Permagon Press, Oxford, 1982 121 pp.
[44] J. Tullis, R.A. Yund, Experimental deformation of dry Westerly granite, J. Geophys. Res. 82 (1977) 5705–5718.
[45] M. Shimada, A. Cho, Two types of brittle fracture of silicate rocks under confining pressure and their implications in the earth's crust, Tectonophysics 175 (1990) 221–235.
[46] G. Hirth, J. Tullis, The brittle-plastic transition in experimentally deformed quartz aggregates, J. Geophys. Res. 99 (1994) 11,731–11,747.
[47] J. Tullis, R. Yund, The brittle–ductile transition in feldspar aggregates: an experimental study, in: B. Evans (Ed.), Fault Mechanics and Transport Properties of Rocks, Academic, San Diego, Calif., 1992, pp. 89–117.
[48] J.V. Ross, K.C. Nielsen, High-temperature flow of wet polycrystalline enstatite, Tectonophysics 44 (1978) 233–261.
[49] F. Birch, Compressibility; elastic constants, in: S.P. Clark (Ed.), Handbook of Physical Constants Memoir, vol. 97, Geol. Soc. Amer, New York, 1966, pp. 107–173.
[50] N.I. Christensen, Poisson's ratio and crustal seismology, J. Geophys. Res., [Solid Earth] 101 (1996) 3139–3156.
[51] J.N. Wang, T.G. Nieh, Effects of the Peierls stress on the transition from power–law creep to Harper–Dorn creep, Acta Metall. Mater. 43 (1995) 1415–1419.
[52] J.N. Wang, Prediction of Peierls stresses for different crystals, Mater. Sci. Eng., A Struct. Mater. Prop. Microstruct. Process. 206 (1996) 259–269.